Geophysical Research Letters

RESEARCH LETTER
10.1029/2025GL121354

On the Utility of the Transient Climate Response

Nadir Jeevanjee[1], D. J. Paynter[1], J. P. Dunne[1], L. T. Sentman[1], and J. P. Krasting[1]

[1]Geophysical Fluid Dynamics Laboratory, Princeton, NJ, USA

Key Points:

- Forcing and temperature are linearly related in transient climate change scenarios by the Transient Climate Response (TCR)
- This linear relationship accurately predicts temperature change over the coming decades given only a forcing projection and a value for TCR
- Deviations from a linear relationship occur on longer timescales due to deep ocean heat uptake and its "efficacy" (i.e., the pattern effect)

Correspondence to:

N. Jeevanjee,
nadir.jeevanjee@noaa.gov

Citation:

Jeevanjee, N., Paynter, D. J., Dunne, J. P., Sentman, L. T., & Krasting, J. P. (2026). On the utility of the Transient Climate Response. *Geophysical Research Letters*, *53*, e2025GL121354. https://doi.org/10.1029/2025GL121354

Received 16 DEC 2025
Accepted 18 MAR 2026

Abstract The Transient Climate Response (TCR) is a metric of climate sensitivity relevant to present-day climate change, but has been less studied than the Equilibrium Climate Sensitivity. Here, we emphasize the utility of the TCR by demonstrating that temperature and radiative forcing in transient scenarios are linearly related, where the proportionality constant is essentially the TCR. This relationship has been invoked in previous studies but not extensively validated; here it is shown to hold across models as well as forcing scenarios. This linear scaling furthermore allows for a simple estimate of the time to cross a given temperature target, given only a forcing scenario and a value for TCR. Deviations from a strictly linear relationship between temperature and forcing are governed by the "slow" component of global warming driven by declining deep ocean heat uptake, but can only be fully accounted for by incorporating changing patterns of surface warming via ocean heat uptake "efficacy."

Plain Language Summary Different measures of climate sensitivity capture different aspects of the Earth's response to increased carbon dioxide. While much attention has been paid to the Equilibrium Climate Sensitivity, another measure of climate sensitivity which is arguably more relevant for present-day climate change is the Transient Climate Response (TCR). Here we demonstrate a general linear relationship between radiative forcing (from carbon dioxide and/or other forcing agents) and surface warming in transient climate change scenarios, where the constant of proportionality is essentially just the TCR. Furthermore, this linear relationship helps us predict when the Earth may cross a specific temperature target. These results highlight the utility of TCR for conceptualizing and predicting near-term climate change.

1. Introduction

Calculating the sensitivity of Earth's climate to CO_2 perturbations is a nontrivial question even to pose, let alone answer, as the answer depends on how the question is asked. In a modeling context, the most straightforward approach is to prescribe a perturbed CO_2 concentration (say, a doubling relative to preindustrial) and calculate the temperature change at equilibrium. Historically, this was done by running atmospheric general circulation models over "mixed-layer" oceans, which only simulate the upper 50–100 m of the world ocean and typically equilibrate within a few decades of model run time. The resulting Equilibrium Climate Sensitivity (ECS) measures the overall magnitude of global warming, and turns out to be a convenient metric for model benchmarking and evaluation (e.g., Charney et al., 1979; Mitchell et al., 1990).

The advent of fully coupled atmosphere-ocean models, however, made it natural to also consider transient, non-equilibrium metrics of climate sensitivity, as coupled models explicitly simulate the deep ocean with its large thermal inertia and thus exhibit a substantial disequilibrium and delay in global warming (Bryan et al., 1982). This phenomenon is captured by "1pctCO2" simulations in which prescribed CO_2 concentrations increase at 1% per year from preindustrial until they double at year 70. The temperature perturbation at this time is known as the Transient Climate Response (TCR) and is significantly less than the ECS, typically by roughly a factor of 2; it too has become a standard for benchmarking and evaluating models (e.g., Meehl et al., 2020).

Despite the greater relevance of TCR for present-day warming, greater attention has been paid to ECS, especially in recent years (Sherwood et al., 2020; Stevens et al., 2016; Zelinka et al., 2020). That same attention, however, has also revealed a number of complications in quantifying and interpreting ECS. For instance, calculating ECS in fully coupled models requires either millennial run times or ambiguous extrapolation from shorter runs (Dunne et al., 2020; Rugenstein et al., 2020). Also, the climate feedbacks relevant for ECS are likely not the same as in a transient scenario due to differences in sea surface temperature (SST) patterns (i.e., the "pattern effect," Andrews et al., 2015; Armour et al., 2013). Finally, ECS by definition includes only the "fast" feedbacks operating in early climate models (Charney et al., 1979) and excludes certain Earth system feedbacks such as changes in

atmospheric composition, vegetation, and ice sheets, which occur over timescales less than or comparable to that required for deep ocean equilibration (Previdi et al., 2013; Rohling et al., 2012).

Given these difficulties with ECS, as well as TCR's natural suitability for capturing the response of models (and ideally the real Earth) to time-dependent radiative forcing, we focus here on highlighting some fundamental properties of TCR and its utility in conceptualizing and predicting near-term climate change. This work builds off the work of Gregory and Forster (2008) as well as the recent review of Jeevanjee et al. (2025), both of which demonstrated in individual models that TCR can be scaled by the radiative forcing to estimate the temperature response across a variety of transient forcing scenarios. Here, we also verify this TCR scaling across models participating in the Radiative Forcing Model Intercomparison Project (RFMIP, Pincus et al., 2016) for which transient forcing output is available. While this scaling is known and has been widely applied to evaluate Earth's TCR from historical observations (de-la Cuesta & Mauritsen, 2019; Lewis & Curry, 2015; Marvel et al., 2016; Nijsse et al., 2020; Otto et al., 2013), the present results instead *validate* the scaling and demonstrate its general applicability across models and scenarios.

We also present a further application of the scaling by using it to estimate the time at which a given temperature threshold (e.g., 1.5°C or 2°C) would be crossed. We conclude by briefly investigating the approximations inherent in the TCR scaling and how these manifest as errors at larger forcing and temperature values. We find that these errors are not fully explained by declining ocean heat uptake unless the SST pattern effect is accounted for via ocean heat uptake "efficacy" (Winton et al., 2010).

Throughout this paper, F will denote the effective radiative forcing (ERF) in $\mathrm{W/m^2/K}$ calculated as the top-of-atmosphere (TOA) net radiation N from simulations with fixed SSTs but time-varying forcing agents (Forster et al., 2016; Hansen et al., 2005). The ERF includes the stratospheric adjustment as well as other adjustments from clouds, water vapor, etc. (Quaas et al., 2024; Sherwood et al., 2015). With F defined this way, any other perturbations to N can be ascribed to surface temperature perturbations T_s, whose impact on N is given by the feedback parameter $\lambda = dN/dT_s < 0$. This then yields the well-known forcing-feedback decomposition at TOA,

$$N = F - |\lambda| T_s, \tag{1}$$

which we will refer to throughout. Note that here λ is assumed constant and in particular cannot vary with SST pattern (the pattern effect is neglected). We will relax this assumption in Section 4.2.

2. TCR Scaling From Mixed-Layer Quasi-Equilibrium

The theoretical foundation for the TCR scaling is the approximation of *mixed-layer quasi-equilibrium* (MLQE), which we briefly review here. The MLQE approximation is discussed in more detail in Jeevanjee et al. (2025) and numerous other references, especially Gregory et al. (2015). As emphasized there, MLQE is a special case of the familiar two-box model (Gregory, 2000; Held et al., 2010):

$$C_s \frac{dT_s}{dt} = F - |\lambda| T_s - \gamma (T_s - T_d) \tag{2a}$$

$$C_d \frac{dT_d}{dt} = \gamma (T_s - T_d). \tag{2b}$$

The first equation describes the energy balance of the ocean mixed layer, whose heat capacity C_s is set by its characteristic depth of approximately 100 m and whose uniform temperature anomaly T_s responds to radiative forcing F by both increasing the net radiation to space by an amount $|\lambda| T_s$ and exporting heat to the deep ocean by an amount $\gamma(T_s - T_d)$, where γ is the ocean heat uptake coefficient in units of $\mathrm{W/m^2/K}$. The second equation describes the energy balance of the deep ocean, whose much larger heat capacity C_d scales with its much greater depth of $3 - 4$ km and whose temperature anomaly T_d responds only to the heat flux from the mixed layer.

Assuming a transient scenario whose timescales of interest are multi-decadal, and that T_s responds on annual timescales while T_d responds on centennial time scales (as per their effective depths, Geoffroy, Saint-Martin, Olivié, et al., 2013; Jeevanjee, 2023), we take the mixed layer heat capacity $C_s \approx 0$ and the deep ocean heat

capacity $C_d \to \infty$, which implies $T_d \equiv 0$ (this is the "zero-layer model" of Gregory et al. (2015)). With these approximations, the mixed-layer energy budget 2a no longer contains a time derivative and instead describes a mixed layer in quasi-equilibrium (MLQE), in which radiative forcing is perfectly balanced by the sum of net radiation to space and heat uptake by the deep ocean. (Note that this heat uptake is actually equal to the TOA net radiation N, since under these assumptions $N = F - |\lambda| T_s = \gamma T_s$.) As $F(t)$ evolves, T_s adjusts instantaneously (thanks to $C_s \approx 0$) to enforce this balance. In this MLQE approximation, T_s is obtained from Equation 2a with $C_s \approx 0$ and $T_d \approx 0$ as

$$T_s \approx \frac{F}{\gamma + |\lambda|} \quad \text{(MLQE)}. \tag{3}$$

In MLQE, then, T_s is proportional to F. This expression can also be obtained from the TOA energy budget 1 assuming also that $N = \gamma T_s$ (Raper et al., 2002), but we prefer to begin from the mixed layer energy budget 2a to make explicit the physical assumptions behind the MLQE approximation, and also because we will need this mixed layer perspective in Section 4.

Equation 3 should apply in particular to a 1pctCO2 simulation and hence to the definition of TCR as the warming at year 70, when the forcing $F_{2\times}$ is that due to a doubling of CO_2 concentrations. Specializing to this case then yields an expression for TCR:

$$\text{TCR} \approx \frac{F_{2\times}}{\gamma + |\lambda|}. \tag{4}$$

If we now combine Equations 3 and 4, we find that we can estimate transient warming in a *generic* transient scenario by scaling the TCR by the time-dependent forcing $F(t)$:

$$T_s(t) \approx \frac{F(t)}{F_{2\times}} \text{TCR} \quad \text{(TCR scaling, transient scenario)}. \tag{5}$$

As referenced in the introduction, this expression is not new and has been used in the past to estimate TCR from observations. At the same time it has not been extensively validated, nor has its generality been fully explored, as the above derivation suggests that Equation 5 should apply to *any* transient scenario over multi-decadal timescales. This implies that for a given TCR, all such scenarios should exhibit the *same* linear relationship between F and T_s (Gregory & Forster, 2008).

To test these ideas, we need coupled simulations of various scenarios to obtain $T_s(t)$ (calculated as global-mean near-surface air temperature), as well as corresponding fixed-SST experiments with time-varying forcing agents to obtain the ERF $F(t)$. Figure 1 shows the results of such simulations with GFDL-CM4 (Held et al., 2019), including runs for the historical/SSP2-4.5 scenario with differing forcing agents, as well as for a 1pctCO2 scenario extended to 140 years to quadrupled CO_2. Figure 1a shows annual and global mean $F(t)$ from the fixed SST runs, Figure 1b shows $T_s(t)$ from the coupled runs, and Figure 1c scatterplots these annual mean, global mean quantities against each other. Figure 1c also shows the TCR scaling 5, using $F_{2\times} = 4.2$ W/m^2/K and TCR = 2.0 K as evaluated over years 60–80 of the 1pctCO2 simulation (similar to the values of Winton et al. (2020)).

The forcing scenarios and temperature responses in Figures 1a and 1b are diverse in slope, shape, and even sign. Despite this diversity, however, all runs exhibit a rather remarkable collapse onto roughly the same quasi-linear curve in Figure 1c. Furthermore, the TCR scaling 5 provides a reasonable approximation to this curve, especially for forcings less than 5 W/m^2 or so. Beyond that the MLQE approximation breaks down, due to effects we will explore in Section 4. In the His-All case, one can also see a few black dots at low T_s values which deviate from the linear scaling; these are precisely the years of large volcanic eruptions (negative spikes in black line in Figure 1a) whose forcings dissipate on time scales shorter than the mixed layer response time and which therefore do not obey MLQE (Gregory & Forster, 2008).

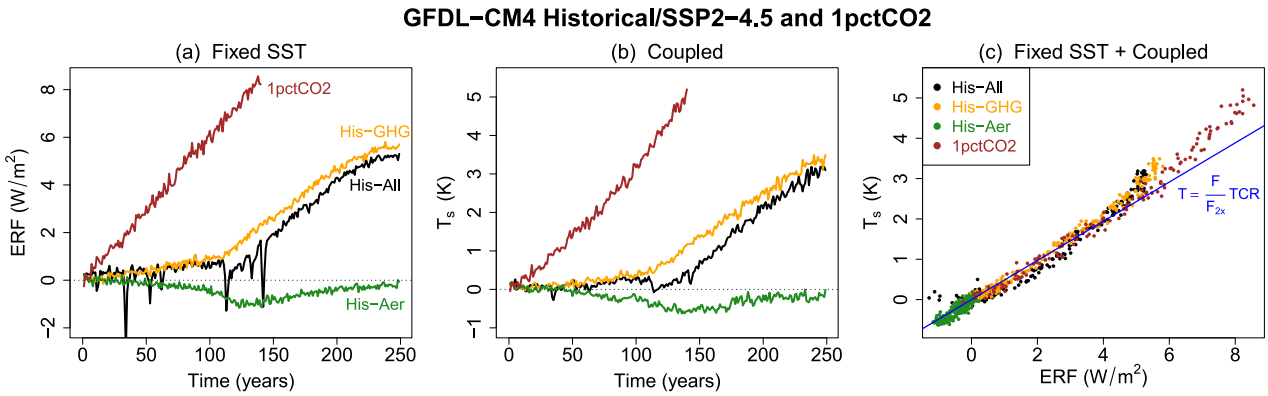

Figure 1. *Effective radiative forcing (ERF), T_s, and Transient Climate Response (TCR) scaling across scenarios* (a) annual mean, global mean ERF $F(t)$ from fixed-sea surface temperature simulations with GFDL-CM4 for variants of the historical/SSP2-4.5 scenario as well as a 1pctCO2 scenario. The His-All scenario includes all forcing agents (anthropogenic and natural), His-GHG includes only greenhouse gases, and His-Aer includes only aerosol forcing. Time axis begins at 1850 CE for all historical/SSP2-4.5 runs (b) $T_s(t)$ for the corresponding fully coupled simulations. (c) Scatterplot of T_s versus F for the same scenarios, along with the TCR scaling 5 (blue line). The various scenarios roughly collapse onto the same curve in the $T_s - F$ plane, which is reasonably approximated by the TCR scaling.

3. TCR Scaling Across the RFMIP Ensemble

Figure 1c shows that the TCR scaling 5 applies across scenarios for a single model, GFDL-CM4. Gregory and Forster (2008) obtained similar results for another model, HadCM3 (Gordon et al., 2000). Establishing the robustness of the TCR scaling, however, requires validation across many models. This has not been feasible in the past because the required ERF calculations have not been widely run or systematically archived. Recently, however, several modeling centers contributed the requisite runs to the RFMIP (Pincus et al., 2016) as part of the sixth Coupled Model Intercomparison Project (CMIP6, Eyring et al., 2016). Historical forcing from RFMIP is shown in Figure 2 for participating models that included the extension to 2100 via the SSP2-4.5 scenario (O'Neill et al., 2016; Riahi et al., 2017).

With multi-model forcings in hand, as well as the corresponding coupled simulations readily available, Figure 3 plots $T_s(t)$ versus $F(t)$ for the participating RFMIP models, similar to Figure 1c except we line plot the data and smooth it using a 20-year running mean. For ease of comparison, we also normalize forcing and temperature by

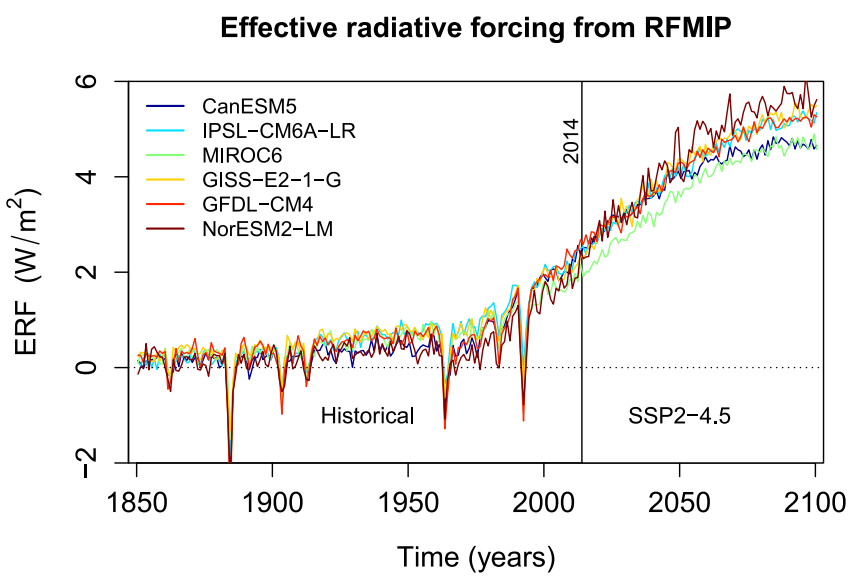

Figure 2. Timeseries of effective radiative forcing for the Historical/SSP2-4.5 scenario for various models, as calculated with fixed-sea surface temperature simulations from models participating in the Radiative Forcing Model Intercomparison Project (Pincus et al., 2016). Ensemble averages are used for models which contributed multiple ensemble members.

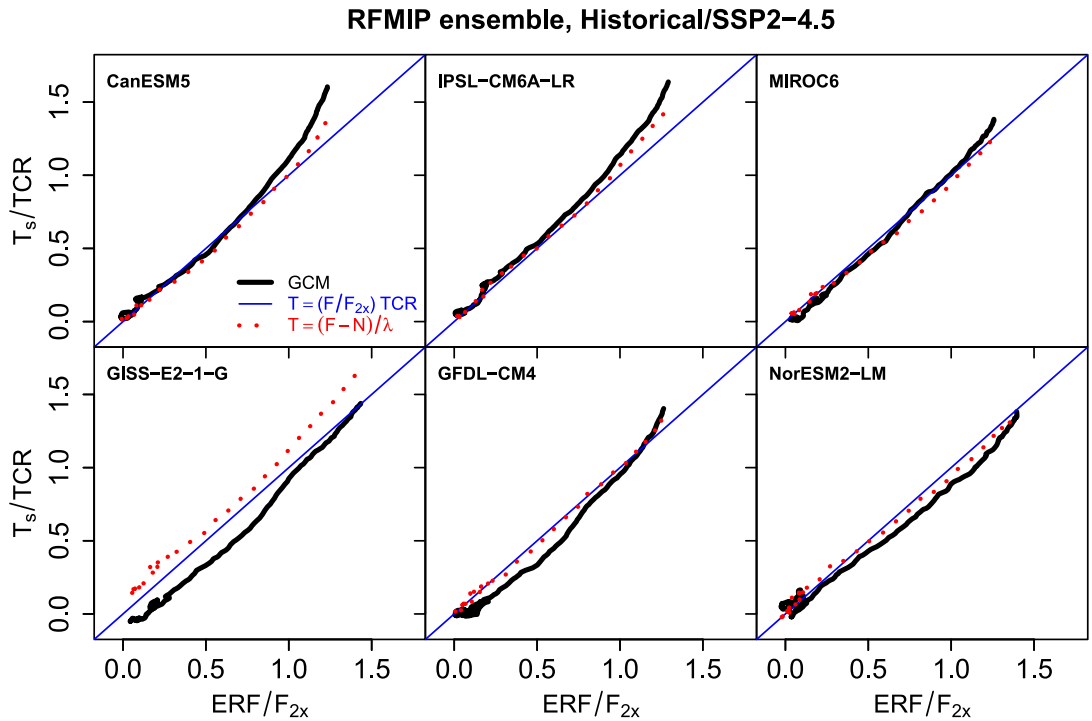

Figure 3. *Testing the proportionality of temperature to forcing across Radiative Forcing Model Intercomparison Project (RFMIP)* Similar to Figure 1c, but for the RFMIP ensemble for the historical/SSP2-4.5 scenario. Here, the annual mean, global mean F, and T_s data are smoothed with a 20-year running mean and line plotted (in black) for clarity. Forcing and temperature are normalized by each model's $F_{2\times}$ and Transient Climate Response for even comparison. As in Figure 1c, the scaling 5 (blue lines) reasonably approximates the simulated evolution over multi-decadal timescales, with some deviation at later times and larger amounts of warming. The dotted red lines show the estimate 8, which captures some but not all curvature for most models (see Section 4).

each model's $F_{2\times}$ and TCR, obtained from published values (Meehl et al., 2020; Smith et al., 2020). As for GFDL-CM4 and HadCM3, there is a roughly linear relationship between $T_s(t)$ and $F(t)$ for each model, which furthermore is approximately captured by the TCR scaling 5 (which with these normalizations is also the 1-1 line, in blue). There are systematic deviations from the TCR scaling at late times due to the breakdown of the MLQE approximation, although the degree of deviation differs among models and the magnitude is not large: the RMSE at year 2100 between the TCR scaling and the simulations, normalized by the ensemble mean T_s/TCR at 2100, is 15%. These deviations, as well as the red dotted lines in this figure, will be discussed in Section 4.

To further validate the TCR scaling across models, as well as provide a practical application of this scaling, we now ask if given a forcing timeseries $F(t)$, can one predict the time at which a given model will cross a given temperature target, for example, 1.5°C or 2°C (UNFCC, 2015). Specifically, given a temperature target T^*, we attempt to estimate the time t* for which $T_s(t^*) = T^*$ by invoking Equation 5 to set

$$F(t^*) = F_{2\times}\frac{T^*}{\mathrm{TCR}} \tag{6}$$

and solving numerically for t^*. The y-axis of Figure 4 shows t^* estimated in this manner for $T^* = 1.5$, 2°C and for each RFMIP model using its TCR, $F_{2\times}$, and Historical/SSP2-4.5 $F(t)$ from Figure 2. The x-axis of Figure 4 shows t^* obtained directly by setting $T_s(t^*) = T^*$ in each models's coupled Historical/SSP2-4.5 runs. (We use the smoothed $F(t)$ and $T_s(t)$ to ensure that t^* is single-valued). The estimated t^* from Equation 6 approximates the directly diagnosed t^* very well, capturing roughly 90% of the variance and with RMSE values of 6.0 and 8.0 years for $T^* = 1.5$ and 2°C, respectively.

The TCR scaling 5 thus appears to contain useful information about climate change in the coming decades. Note that the results of Figure 1 suggest that this utility of TCR should be relatively robust across scenarios and the time

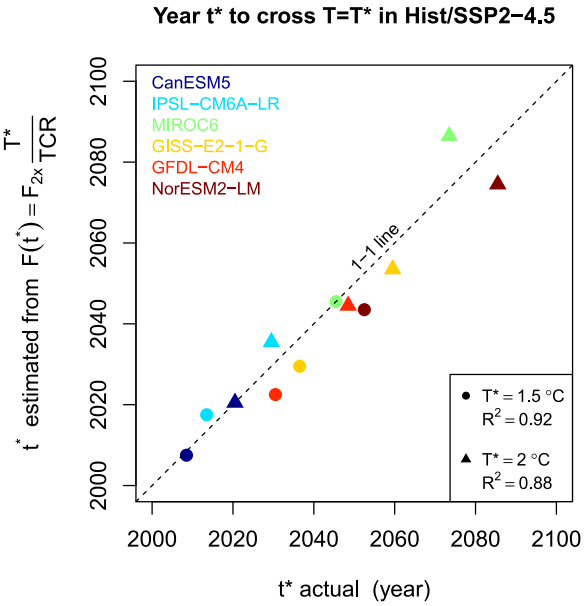

Figure 4. *Time* t^* in a Historical/SSP2-4.5 scenario at which a temperature target of 1.5°C (circles) or 2°C (triangles) is exceeded, as diagnosed directly from coupled simulations (x-axis) or as estimated from Equation 6 (y-axis). The latter estimate uses only a given model's Transient Climate Response (TCR) and $F(t)$ from Figure 2. The strong correlation between the diagnosed and estimated t^* highlights the utility of TCR in predicting near-term, transient climate change.

evolution of different forcing agents, rather than strongly contingent on specific aspects of the SSP2-4.5 scenario (although see Section 5 for further discussion). It is also worth noting that the dashed line in Figure 4 is not a best-fit line or emergent constraint as in prior works (de-la Cuesta & Maurtisen, 2019; Nijsse et al., 2020); rather, it is the 1-to-1 line produced by an a priori constraint obtained from theoretical considerations. Furthermore, estimating t^* from Equation 6 requires only the TCR and a projection of the forcing, so that the TCR—a single number—is the only information required from coupled model runs.

4. Curvature in the T_s Versus F Relationship

The results so far underscore the utility of the TCR scaling 5, but at the same time, it is evident from Figures 1c and 3 that the linear relationship between T_s and F breaks down and develops curvature at late times and large forcings. In this section, we investigate potential causes for this. This question was also investigated across CMIP5 models in Gregory et al. (2015); we briefly compare our methodology and results with theirs in Section 5.

4.1. The Mixed-Layer Perspective

To understand this curvature we return to the two-box model 2a and 2b and relax the $C_d = \infty$, $T_d \equiv 0$ assumption while retaining $C_s \approx 0$. Since $C_s \approx 0$ we still have N equal to the deep ocean heat uptake, only now as

$$N = F - |\lambda| T_s = \gamma (T_s - T_d). \tag{7}$$

Since deep ocean heat uptake removes heat from the mixed layer, N can be considered a negative "forcing" from the mixed layer perspective. We can express this by rewriting the mixed layer energy budget 2a (or equivalently the TOA balance 1) as

$$T_s = \frac{F}{|\lambda|} - \frac{N}{|\lambda|}, \tag{8}$$

expressing T_s as the sum of warming from the (positive) TOA radiative forcing F and cooling from the (negative) deep ocean heat uptake $-N$ (Rose & Rayborn, 2016). By Equation 7 we see that over time N will decline relative to its $T_d = 0$ value of γT_s; this decline is precisely what yields the "slow" component of warming identified by Held et al. (2010), by decreasing the magnitude of the $-N$ term on the right side of Equation 8. Note that we need not model N itself (say, using the two-box model) to assess whether this decline in deep ocean heat uptake yields curvature in T_s versus F; instead, we may simply diagnose N from the simulations and test how well Equation 8 captures the simulated T_s versus F.

This is shown by the dotted red lines in Figure 3 for our RFMIP simulations (λ is obtained by solving Equation 8 for λ and evaluating at CO_2 doubling in each models' respective 1pctCO2 simulations). For all models besides GISS-E2-1-G, for which the estimate 8 exhibits a significant but relatively constant offset, the simulations exhibit more curvature than the estimate 8, which itself more closely follows the linear estimate 5. Thus, relaxing the $T_d = 0$ assumption of the MLQE approximation is by itself insufficient to capture the curvature in T_s versus F. The next obvious culprit is the pattern effect, which we turn to next.

4.2. Ocean Heat Uptake Efficacy in GFDL-CM4

The "pattern effect" is a generic term which refers to the dependence of λ on the spatial pattern of SST change, which can lead to a time dependence of λ and which has various implications for understanding historical and projected warming (Andrews et al., 2015; Armour et al., 2013; Lee et al., 2022; Rugenstein et al., 2023). Here we follow Winton et al. (2010) and Rose and Rayborn (2016) and invoke the pattern effect in the context of the mixed-layer perspective 8, where the pattern effect manifests not as a time dependence in a single feedback

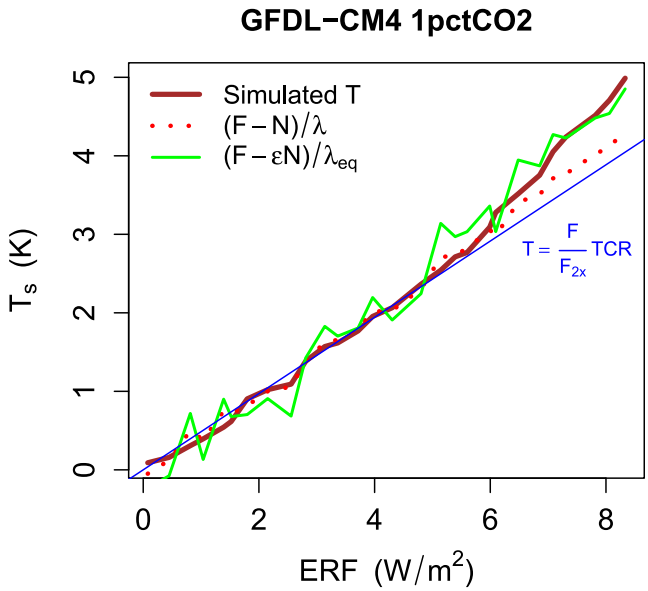

Figure 5. *Ocean heat uptake efficacy captures curvature in T_s versus* F *for GFDL-CM4* Simulated T_s versus F in brown, using the same data as Figure 1c but with a 5-year running mean. Significant curvature is visible at large F and T_s. Incorporating the impacts of deep ocean warming (Equation 8, dotted red line) generates only slight curvature, whereas incorporating the sea surface temperature pattern effect via ocean heat uptake efficacy (Equation 9, green line) yields a good match.

parameter but rather as a *difference* in the feedback parameters associated to the two mixed-layer forcings F and N, justified by the fact that N acts primarily at high latitudes and thus induces a different pattern of SST anomalies than F (Winton et al., 2010). This difference in λ can equivalently be viewed as a difference in the "efficacy" of these two forcings (Haugstad et al., 2017; Winton et al., 2010; Zhou et al., 2023). We thus generalize Equation 8 to

$$T_s(t) = \frac{F}{|\lambda_{eq}|} - \frac{\varepsilon N}{|\lambda_{eq}|} \tag{9}$$

where λ_{eq} is now the *equilibrium* feedback parameter associated with F (as it must be in the $N \to 0$ limit) and λ_{eq}/ε is the feedback parameter associated with N, where ε is the heat uptake efficacy. Since ε is typically greater than 1 (Winton et al., 2010), any relative decline in N has a greater impact in Equation 9 than in Equation 8; in this way heat uptake efficacy "amplifies" the slow component of warming.

We now test the accuracy of Equation 9 in the context of the GFDL-CM4 1pctCO2 simulation, where we take $|\lambda_{eq}| = F_{2\times}/\mathrm{ECS}$ and ECS = 5.0 K is derived from a 300-year abrupt4x simulation (Winton et al., 2020). Evaluating Equation 9 at CO_2 doubling yields $\varepsilon = 1.84$. With these parameters, Figure 5 then line plots $T_s(t)$ versus $F(t)$ from the simulation and as estimated from Equations 8 and 9, with a 5-year running mean applied. Again, we see that the estimate 8 has insufficient curvature and tracks the linear TCR scaling 5 fairly closely. On the other hand, the estimate 9 which includes the heat uptake efficacy does fairly well, capturing the curvature at late times. This shows that ocean heat uptake efficacy (and thus the pattern effect) plays a significant role in the curvature of the T_s versus F relationship for GFDL-CM4.

What about the curvature seen in T_s versus F for the RFMIP models in Figure 3? In principle, the above analysis could also be performed for the RFMIP ensemble, but precise estimates of ECS and hence λ_{eq} are not obtainable from the standard 150 years abrupt4x simulations (Dunne et al., 2020). Furthermore, the historical/SSP2-4.5 scenario utilized in RFMIP includes non-CO_2 forcing agents which may also require their own efficacy, requiring elaboration of Equation 9 (Marvel et al., 2016). Indeed, the His-All run shown in Figure 1c has less warming at $F \approx 2 - 3$ W/m^2/K than the His-GHG or 1pctCO2 runs, and the best-fit slope of the His-Aer data in Figure 1c is actually slightly larger than TCR/$F_{2\times}$, by 20%; all of this points to an aerosol forcing efficacy greater than unity in GFDL-CM4 (Winton et al., 2020).

5. Conclusions

This work has shown that:

- The linear relationship 5 between temperature anomaly T_s and effective radiative forcing F holds across scenarios and models (Figures 1 and 3)
- This linear TCR scaling can be used to predict the time to cross a given temperature threshold (Figure 4)
- Deviations from the linear TCR scaling cannot be captured by the slow component of warming without also accounting for amplification by the pattern effect, as encapsulated here by non-unit ocean heat uptake efficacy (Figures 3 and 5, Equation 9)

This last conclusion above differs from that of prior studies. For instance, Gregory et al. (2015) and Geoffroy, Saint-Martin, Bellon, et al. (2013) both found a minimal role for the pattern effect in producing deviations from the linear TCR scaling. Both these studies relied on emulators, however—a linear response model in the case of Gregory et al. (2015), and the two-box model in the case of Geoffroy, Saint-Martin, Bellon, et al. (2013). Here, we leveraged recent RFMIP output and protocols to more directly assess the role of the pattern effect, by applying Equations 8 and 9 directly to climate model output.

An outstanding question we have not addressed is exactly when and under what scenarios we expect the MLQE approximation 3 and ensuing TCR scaling 5 to break down. In Figure 1c this breakdown begins at roughly $(F, T_s) = \left(5\ \mathrm{W/m^2/K},\ 2.5\ \mathrm{K}\right)$ for the 1pctCO2 scenario, and at perhaps slightly smaller values for His-all and His-GHG. One might expect the breakdown to occur somewhat earlier for scenarios where the forcing stabilizes or decreases, such as SSP1-2.6 (O'Neill et al., 2016); in such scenarios the slow component will increase in relevance earlier on, breaking the linearity between T_s and F at earlier times and smaller perturbation levels. Future work could include ERF calculations for such scenarios to facilitate a more general evaluation of the MLQE approximation and TCR scaling.

Another caveat is that while this work has attempted to illustrate the utility of TCR in conceptualizing and predicting near-term climate change, previous works have of course also conveyed this message (Allen et al., 2022; Andrews et al., 2012; Knutti et al., 2017, see also https://www.gfdl.noaa.gov/blog_held/51-the-simplest-diffusive-model-of-oceanic-heat-uptake-and-tcr/). Here, we have illustrated the utility of TCR using comprehensive coupled models combined with newly available forcing calculations.

Finally, it is notable how well the simple parameterization 9 captures the evolution of the GFDL-CM4 1pctCO2 simulation in Figure 5. A similar fit was also shown for an abrupt4x simulation of an earlier model, GFDL-CM2.1, in Winton et al. (2010). This speaks to the utility of the mixed-layer perspective (Equations 8 and 9) in understanding *transient* climate change, just as the TOA perspective 1 is critical for understanding equilibrium climate change. It may be the case that different paradigms are required for understanding these various regimes of climate change.

Conflict of Interest

The authors declare no conflicts of interest relevant to this study.

Availability Statement

Reduced data and scripts for producing the figures in this paper are available at https://zenodo.org/records/17956474 (Jeevanjee et al., 2026).

Acknowledgments
The authors thank Jing Feng and Tim Merlis for internal reviews of drafts of this work, and Cristian Proistosescu and an anonymous reviewer for helpful feedback on the initial submission.

References

Allen, M. R., Friedlingstein, P., Girardin, C. A., Jenkins, S., Malhi, Y., Mitchell-Larson, E., et al. (2022). Net zero: Science, origins, and implications. *Annual Review of Environment and Resources*, *47*(1), 849–887. https://doi.org/10.1146/annurev-environ-112320-105050

Andrews, T., Gregory, J. M., & Webb, M. J. (2015). The dependence of radiative forcing and feedback on evolving patterns of surface temperature change in climate models. *Journal of Climate*, *28*(4), 1630–1648. https://doi.org/10.1175/JCLI-D-14-00545.1

Andrews, T., Gregory, J. M., Webb, M. J., & Taylor, K. E. (2012). Forcing, feedbacks and climate sensitivity in CMIP5 coupled atmosphere-ocean climate models. *Geophysical Research Letters*, *39*(9), L09712. https://doi.org/10.1029/2012GL051607

Armour, K. C., Bitz, C. M., & Roe, G. H. (2013). Time-varying climate sensitivity from regional feedbacks. *Journal of Climate*, *26*(13), 4518–4534. https://doi.org/10.1175/JCLI-D-12-00544.1

Bryan, K., Komro, F. G., Manabe, S., & Spelman, M. J. (1982). Transient climate response to increasing atmospheric carbon dioxide. *Science*, *215*(4528), 56–58. https://doi.org/10.1126/science.215.4528.56

Charney, J., Arakawa, A., Baker, D. J., Bolin, B., Dickinson, R. E., Goody, R. M., et al. (1979). *Carbon dioxide and climate: A scientific assessment (Tech. Rep.)*. National Academy of Sciences. Retrieved from http://www.cs.toronto.edu/~sme/CSC2602/CharneyReportPresentation_Pif.pdf

de-la Cuesta, D. J., & Mauritsen, T. (2019). Emergent constraints on Earth's transient and equilibrium response to doubled CO_2 from post-1970s global warming. *Nature Geoscience*, *12*(11), 902–905. https://doi.org/10.1038/s41561-019-0463-y

Dunne, J. P., Winton, M., Bacmeister, J., Danabasoglu, G., Gettelman, A., Golaz, J. C., et al. (2020). Comparison of equilibrium climate sensitivity estimates from slab ocean, 150-year, and longer simulations. *Geophysical Research Letters*, *47*(16), e2020GL088852. https://doi.org/10.1029/2020GL088852

Eyring, V., Bony, S., Meehl, G. A., Senior, C. A., Stevens, B., Stouffer, R. J., & Taylor, K. E. (2016). Overview of the coupled model intercomparison project phase 6 (CMIP6) experimental design and organization. *Geoscientific Model Development*, *9*(5), 1937–1958. https://doi.org/10.5194/gmd-9-1937-2016

Forster, P. M., Richardson, T., Maycock, A. C., Smith, C. J., Samset, B. H., Myhre, G., et al. (2016). Recommendations for diagnosing effective radiative forcing from climate models for CMIP6. *Journal of Geophysical Research: Atmospheres*, *121*(20), 12460–12475. https://doi.org/10.1002/2016JD025320

Geoffroy, O., Saint-Martin, D., Bellon, G., Voldoire, A., Olivié, D. J., & Tytéca, S. (2013). Transient climate response in a two-layer energy-balance model. Part ii: Representation of the efficacy of deep-ocean heat uptake and validation for CMIP5 AOGCMs. *Journal of Climate*, *26*(6), 1859–1876. https://doi.org/10.1175/JCLI-D-12-00196.1

Geoffroy, O., Saint-Martin, D., Olivié, D. J., Voldoire, A., Bellon, G., & Tytéca, S. (2013). Transient climate response in a two-layer energy-balance model. Part i: Analytical solution and parameter calibration using CMIP5 AOGCM experiments. *Journal of Climate*, *26*(6), 1841–1857. https://doi.org/10.1175/JCLI-D-12-00195.1

Gordon, C., Cooper, C., Senior, C. A., Banks, H., Gregory, J. M., Johns, T. C., et al. (2000). The simulation of SST, sea ice extents and ocean heat transports in a version of the Hadley Centre coupled model without flux adjustments. *Climate Dynamics*, *16*(2–3), 147–168. https://doi.org/10.1007/s003820050010

Gregory, J. M. (2000). Vertical heat transports in the ocean and their effect on time-dependent climate change. *Climate Dynamics*, *16*(7), 501–515. https://doi.org/10.1007/s003820000059

Gregory, J. M., Andrews, T., & Good, P. (2015). The inconstancy of the transient climate response parameter under increasing CO_2. *Philosophical Transactions of the Royal Society A: Mathematical, Physical and Engineering Sciences*, *A373*(2054), 20140417. https://doi.org/10.1098/rsta.2014.0417

Gregory, J. M., & Forster, P. M. (2008). Transient climate response estimated from radiative forcing and observed temperature change. *Journal of Geophysical Research*, *113*(D23), 1–15. https://doi.org/10.1029/2008JD010405

Hansen, J., Sato, M., Ruedy, R., Nazarenko, L., Lacis, A., Schmidt, G. A., et al. (2005). Efficacy of climate forcings. *Journal of Geophysical Research*, *110*(D18), 1–45. https://doi.org/10.1029/2005JD005776

Haugstad, A. D., Armour, K. C., Battisti, D. S., & Rose, B. E. (2017). Relative roles of surface temperature and climate forcing patterns in the inconstancy of radiative feedbacks. *Geophysical Research Letters*, *44*(14), 7455–7463. https://doi.org/10.1002/2017GL074372

Held, I. M., Guo, H., Adcroft, A., Dunne, J. P., Horowitz, L. W., Krasting, J., et al. (2019). Structure and performance of GFDL's CM4.0 climate model. *Journal of Advances in Modeling Earth Systems*, *11*(11), 1–37. https://doi.org/10.1029/2019ms001829

Held, I. M., Winton, M., Takahashi, K., Delworth, T., Zeng, F., & Vallis, G. K. (2010). Probing the fast and slow components of global warming by returning abruptly to preindustrial forcing. *Journal of Climate*, *23*(9), 2418–2427. https://doi.org/10.1175/2009JCLI3466.1

Jeevanjee, N. (2023). Climate sensitivity from radiative-convective equilibrium: A chalkboard approach. *American Journal of Physics*, *91*(9), 731–745. https://doi.org/10.1119/5.0135727

Jeevanjee, N., Paynter, D., Dunne, J., Sentman, L., & Krasting, J. (2026). Data for 'on the utility of the transient climate response'. Retrieved from https://zenodo.org/records/17956474

Jeevanjee, N., Paynter, D. J., Dunne, J. P., Sentman, L. T., & Krasting, J. P. (2025). A holistic view of climate sensitivity. *Annual Review of Earth and Planetary Sciences*, *53*(1), 367–396. https://doi.org/10.1146/annurev-earth-040523-014302

Knutti, R., Rugenstein, M., & Hegerl, G. C. (2017). Beyond equilibrium climate sensitivity. *Nature Geoscience*, *10*, 727–736. https://doi.org/10.1038/NGEO3017

Lee, S., L'Heureux, M., Wittenberg, A. T., Seager, R., O'Gorman, P. A., & Johnson, N. C. (2022). On the future zonal contrasts of equatorial Pacific climate: Perspectives from observations, simulations, and theories. *npj Climate and Atmospheric Science*, *5*(1), 82. https://doi.org/10.1038/s41612-022-00301-2

Lewis, N., & Curry, J. A. (2015). The implications for climate sensitivity of AR5 forcing and heat uptake estimates. *Climate Dynamics*, *45*(3–4), 1009–1023. https://doi.org/10.1007/s00382-014-2342-y

Marvel, K., Schmidt, G. A., Miller, R. L., & Nazarenko, L. S. (2016). Implications for climate sensitivity from the response to individual forcings. *Nature Climate Change*, *6*(4), 386–389. https://doi.org/10.1038/nclimate2888

Meehl, G. A., Senior, C. A., Eyring, V., Flato, G., Lamarque, J. F., Stouffer, R. J., et al. (2020). Context for interpreting equilibrium climate sensitivity and transient climate response from the CMIP6 Earth system models. *Science Advances*, *6*(26), 1–11. https://doi.org/10.1126/sciadv.aba1981

Mitchell, J., Manabe, S., Meleshko, V., & Tokioka, T. (1990). Equilibrium climate change - And its implications for the future. *Climate Change: The IPCC Scientific Assessment*, *131*, 172.

Nijsse, F., Cox, P., & Williamson, M. (2020). An emergent constraint on transient climate response from simulated historical warming in CMIP6 models. *Earth System Dynamics Discussions*, 1–14. https://doi.org/10.5194/esd-2019-86

O'Neill, B. C., Tebaldi, C., Vuuren, D. P. V., Eyring, V., Friedlingstein, P., Hurtt, G., et al. (2016). The scenario model intercomparison project (ScenarioMIP) for CMIP6. *Geoscientific Model Development*, *9*, 3461–3482. https://doi.org/10.5194/gmd-9-3461-2016

Otto, A., Otto, F. E., Boucher, O., Church, J., Hegerl, G., Forster, P. M., et al. (2013). Energy budget constraints on climate response. *Nature Geoscience*, *6*, 415–416. https://doi.org/10.1038/ngeo1836

Pincus, R., Forster, P. M., & Stevens, B. (2016). The radiative forcing model intercomparison project (RFMIP): Experimental protocol for CMIP6. *Geoscientific Model Development*, *9*, 3447–3460. https://doi.org/10.5194/gmd-9-3447-2016

Previdi, M., Liepert, B. G., Peteet, D., Hansen, J., Beerling, D. J., Broccoli, A. J., et al. (2013). Climate sensitivity in the anthropocene. *Quarterly Journal of the Royal Meteorological Society*, *139*(674), 1121–1131. https://doi.org/10.1002/qj.2165

Quaas, J., Andrews, T., Bellouin, N., Block, K., Boucher, O., Ceppi, P., et al. (2024). Adjustments to climate perturbations—mechanisms, implications, observational constraints. *AGU Advances*, *5*, 1–22. https://doi.org/10.1029/2023AV001144

Raper, S. C., Gregory, J. M., & Stouffer, R. J. (2002). The role of climate sensitivity and ocean heat uptake on AOGCM transient temperature response. *Journal of Climate*, *15*, 124–130. https://doi.org/10.1175/1520-0442(2002)015⟨0124:trocsa⟩2.0.co;2

Riahi, K., van Vuuren, D. P., Kriegler, E., Edmonds, J., O'Neill, B. C., Fujimori, S., et al. (2017). The shared socioeconomic pathways and their energy, land use, and greenhouse gas emissions implications: An overview. *Global Environmental Change*, *42*, 153–168. https://doi.org/10.1016/j.gloenvcha.2016.05.009

Rohling, E. J., Sluijs, A., Dijkstra, H. A., Köhler, P., Wal, R. S. V. D., Heydt, A. S. V. D., & Zeebe, R. E. (2012). Making sense of palaeoclimate sensitivity. *Nature*, *491*, 683–691. https://doi.org/10.1038/nature11574

Rose, B. E. J., & Rayborn, L. (2016). The effects of ocean heat uptake on transient climate sensitivity. *Current Climate Change Reports*, *2*(4), 1–12. https://doi.org/10.1007/s40641-016-0048-4

Rugenstein, M., Bloch-Johnson, J., Gregory, J., Andrews, T., Mauritsen, T., Li, C., et al. (2020). Equilibrium climate sensitivity estimated by equilibrating climate models. *Geophysical Research Letters*, *47*(4), 1–12. https://doi.org/10.1029/2019GL083898

Rugenstein, M., Zelinka, M., Karnauskas, K., Ceppi, P., & Andrews, T. (2023). Patterns of surface warming matter for climate sensitivity. *Eos*, *104*, 1–11. https://doi.org/10.1029/2023eo230411

Sherwood, S. C., Bony, S., Boucher, O., Bretherton, C. S., Forster, P. M., Gregory, J. M., & Stevens, B. (2015). Adjustments in the forcing-feedback framework for understanding climate change. *Bulletin of the American Meteorological Society*, *96*(2), 217–228. https://doi.org/10.1175/BAMS-D-13-00167.1

Sherwood, S. C., Webb, M. J., Annan, J. D., Armour, K. C., Forster, P. M., Hargreaves, J. C., et al. (2020). An assessment of Earth's climate sensitivity using multiple lines of evidence. *Reviews of Geophysics*, *58*(4), 1–92. https://doi.org/10.1029/2019rg000678

Smith, C. J., Kramer, R. J., Myhre, G., Alterskjr, K., Collins, W., Sima, A., et al. (2020). Effective radiative forcing and adjustments in CMIP6 models. *Atmospheric Chemistry and Physics*, *20*(16), 9591–9618. https://doi.org/10.5194/acp-20-9591-2020

Stevens, B., Sherwood, S. C., Bony, S., & Webb, M. J. (2016). Prospects for narrowing bounds on Earth's equilibrium climate sensitivity. *Earth's Future*, *4*(11), 512–522. https://doi.org/10.1002/2016EF000376

UNFCC. (2015). Paris agreement to the United Nations framework convention on climate change.
Winton, M., Adcroft, A., Dunne, J. P., Held, I. M., Shevliakova, E., Zhao, M., et al. (2020). Climate sensitivity of GFDL's CM4.0. *Journal of Advances in Modeling Earth Systems*, *12*, 1–17. https://doi.org/10.1029/2019MS001838
Winton, M., Takahashi, K., & Held, I. M. (2010). Importance of ocean heat uptake efficacy to transient climate change. *Journal of Climate*, *23*(9), 2333–2344. https://doi.org/10.1175/2009JCLI3139.1
Zelinka, M. D., Myers, T. A., McCoy, D. T., Po-Chedley, S., Caldwell, P. M., Ceppi, P., et al. (2020). Causes of higher climate sensitivity in CMIP6 models. *Geophysical Research Letters*, *47*, 1–22. https://doi.org/10.1029/2019GL085782
Zhou, C., Wang, M., Zelinka, M. D., Liu, Y., Dong, Y., & Armour, K. C. (2023). Explaining forcing efficacy with pattern effect and state dependence. *Geophysical Research Letters*, *50*(3), 1–9. https://doi.org/10.1029/2022GL101700